Supplemental Information for

Quaternary dynamics of αB-crystallin as a direct consequence of localised tertiary fluctuations in the C-terminus

Andrew J. Baldwin[1], Gillian R. Hilton[2], Hadi Lioe[2], Claire Bagnéris[3], Justin L.P. Benesch[2], Leawis E. Kay[1]

Derivation of Eq. 1 of the text

Consider first the following equilibrium, $A \underset{k_{BA}}{\overset{k_{AB}}{\rightleftarrows}} B \underset{k_{CB}}{\overset{k_{BC}}{\rightleftarrows}} C$, with k_{AB}=k_{CB}=10 s^{-1} and k_{BA}=k_{BC}=100 s^{-1}. The corresponding free energy landscape is shown below (black),

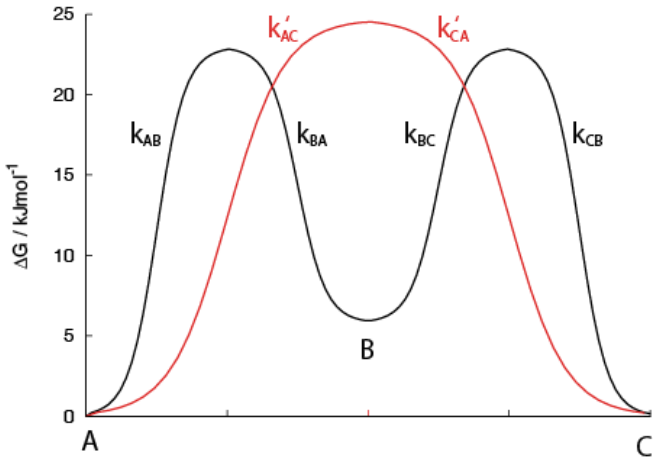

We can write,

$$\frac{d[A]}{dt} = -k_{AB}[A] + k_{BA}[B] \qquad \text{(A1.1)}$$

$$\frac{d[B]}{dt} = k_{AB}[A] - k_{BA}[B] + k_{CB}[C] - k_{BC}[B] \qquad \text{(A1.2)}$$

$$\frac{d[C]}{dt} = -k_{CB}[C] + k_{BC}[B] \qquad \text{(A1.3)}$$

In the steady state limit (equilibrium conditions, or when the population of state B is much lower than that of A or C) $\frac{d[B]}{dt} = 0$ so that $[B] = \frac{k_{AB}[A] + k_{CB}[C]}{k_{BA} + k_{BC}}$. Substituting this into the expression for $\frac{d[C]}{dt}$ above gives:

$$\frac{d[C]}{dt} = -\frac{k_{CB}k_{BA}}{k_{BA} + k_{BC}}[C] + \frac{k_{AB}k_{BC}}{k_{BA} + k_{BC}}[A] \qquad \text{(A1.4)}$$

Thus, if one were to 'model' this three-state process as a two-step equilibrium, $A \underset{k'_{CA}}{\overset{k'_{AC}}{\rightleftarrows}} C$, (as shown by the 'red' profile above) with

$$\frac{d[C]}{dt} = -k'_{CA}[C] + k'_{AC}[A] \qquad \text{(A1.5)}$$

it follows from Eqn. A1.4 that

$$k'_{AC} = \frac{k_{AB}k_{BC}}{k_{BA} + k_{BC}} \qquad \text{(A1.6)}$$

$$k'_{CA} = \frac{k_{CB}k_{BA}}{k_{BA} + k_{BC}} \qquad \text{(A1.7)}$$

From Eqs. (A1.6) and (A1.7) it is clear that $k'_{AC} < k_{AB}, k_{BC}$ and that $k'_{CA} < k_{BA}, k_{CB}$ (see above figure). Thus the 3-state energy landscape is more rugged, with individual activation barriers lower than the 'equivalent' 2-state profile. Starting from the 'Bound, Unpaired' state of Fig. S3B, and using Eq. (A1.6), the rate constant for removal of both flaps is given by $\frac{k^-_{flap}k^-_{flap}}{(k^-_{flap} + k^+_{flap})}$ which we have shown to be equal to k^-_e (Figure 4A).

The rates, k^-_e, k^-_{e+d} and $k^+[P_1]$, derived from the MS measurements can be related to the microscopic NMR rates k^+_{flap} and k^-_{flap} using the results of the derivation above

$$k^-_e = \frac{k^-_{flap}k^-_{flap}}{k^-_{flap} + k^+_{flap}} \qquad \text{(A1.8)}$$

$$k_{e+d}^{-} = k_{e}^{-} \exp\left(\frac{\Delta G_d}{RT}\right) \quad \text{(A1.9)}$$

$$\Delta G_e = -RT \ln \frac{k^{+}[P_1]}{k_e^{-}} \quad \text{(A1.10)}$$

$$\Delta G_{e+d} = -RT \ln \frac{k^{+}[P_1]}{k_{e+d}^{-}} \quad \text{(A1.11)}$$

The microscopic association constant, $k_{\text{int}}^{+}[P_1]$, in Figure 4B and Figure S3 is given by

$$k_{\text{int}}^{+}[P_1] = k^{+}[P_1] \frac{k_{flap}^{+} + k_{flap}^{-}}{k_{flap}^{+}} \quad \text{(A1.12)}$$

following along the same lines as for the derivation of k_e^{-} in terms of k_{flap}^{-} and k_{flap}^{+} above. Here $k_{\text{int}}^{+}[P_1]$ is the pseudo first order rate constant for the formation of the 'intermediate' state where the incoming monomer is held to the oligomer by a single C-terminal interaction.

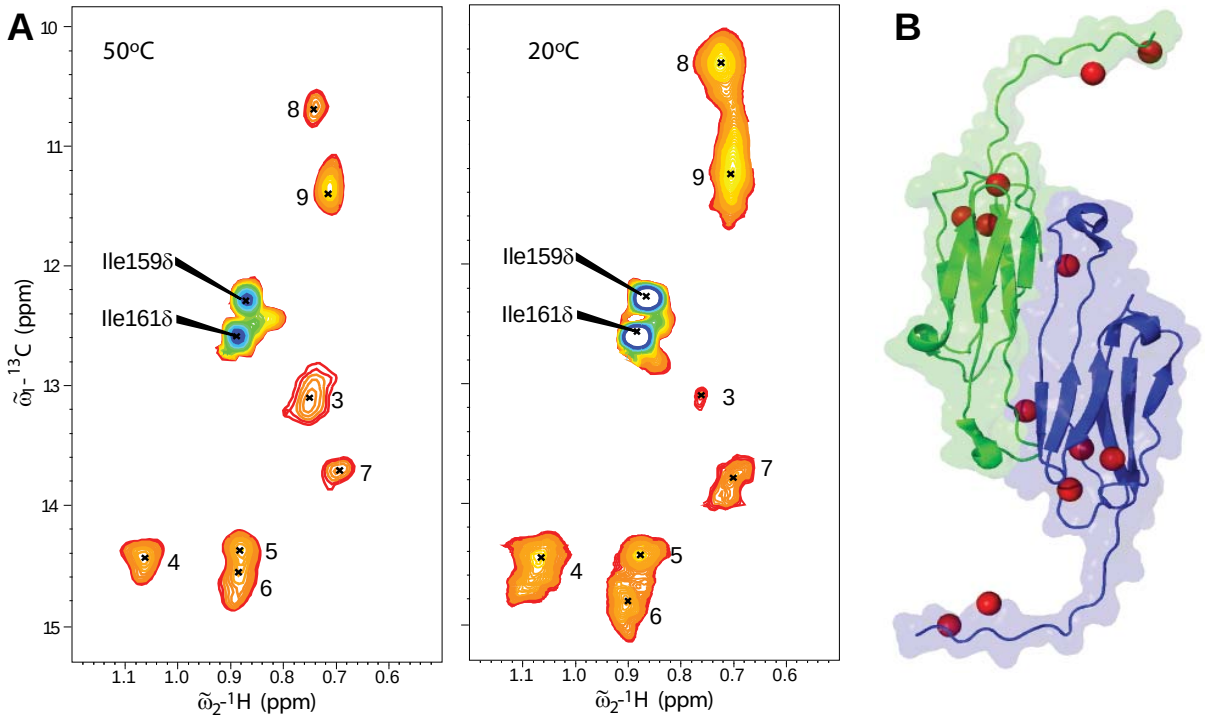

Figure S1. ^{1}H-^{13}C methylTROSY correlation spectra of U-^{2}H,Ile-[^{13}CH$_3$-δ1] labelled αB-crystallin as a function of temperature. **A** – MethylTROSY spectra at 50°C and 20°C. The intensity of the resonances from Ile159 and 161 decrease with temperature due to exchange effects as discussed in the text. By contrast, the remaining relatively broad resonances become more intense with temperature, consistent with the reduction in overall correlation time of the molecule that comes with increased thermal energy. The peak positions do not vary significantly, demonstrating that the hydrophobic core of the protein does not undergo a substantial rearrangement as the ambient temperature is raised. **B** - The locations of the Ile δ1methyl groups are indicated on the dimeric structure of a truncated αB-cystallin (1). Isoleucine side chains are found both on the dimeric interface and within the β-sheet core of the monomers.

```
UniProtKB
Accession  Entry name                                                                  S135        N146
|P02511|CRYAB_HUMAN  68 MRLEKDRFSVNLDVKHFSPEELKVKVLGDVIEVHGKHEERQDEHGFISREFHRKYRIPADVDPLTITSSLSSDGVLTVNGP 148
|Q5R9K0|CRYAB_PONAB  68 MRLEKDRFSVNLDVKHFSPEELKVKVLGDVIEVHGKHEERQDEHGFISREFHRKYRIPADVDPLTITSSLSSDGVLTVNGP 148
|Q60HG8|CRYAB_MACFA  68 MRLEKDRFSVNLDVKHFSPEELKVKVLGDVIEVHGKHEERQDEHGFISREFHRKYRVPADVDPLTITSSLSSDGVLTVNGP 148
|P41316|CRYAB_RABIT  68 MRLEKDRFSVNLDVKHFSPEELKVKVLGDVIEVHGKHEERQDEHGFISREFHRKYRIPADVDPLTITSSLSSDGVLTVNGP 148
|P05811|CRYAB_MESAU  68 MRMEKDRFSVNLDVKHFSPEELKVKVLGDVVEVHGKHEERQDEHGFISREFHRKYRIPADVDPLTITSSLSSDGVLTVNGP 148
|P23928|CRYAB_RAT    68 MRMEKDRFSVNLDVKHFSPEELKVKVLGDVIEVHGKHEERQDEHGFISREFHRKYRIPADVDPLTITSSLSSDGVLTVNGP 148
|Q9EPF3|CRYAB_SPAJD  68 MRMEKDRLSVNLDVKHFSPEELKVKVLGDVIEVHGKHEERQDEHGFISREFHRKYRIPADVDPLTITSSLSSDGVLTVNGP 148
|P23927|CRYAB_MOUSE  68 MRLEKDRFSVNLDVKHFSPEELKVKVLGDVIEVHGKHEERQDEHGFISREFHRKYRIPADVDPLTITSSLSSDGVLTVNGP 148
|P02510|CRYAB_BOVIN  68 MRLEKDRFSVNLDVKHFSPEELKVKVLGDVIEVHGKHEERQDEHGFISREFHRKYRIPADVDPLAITSSLSSDGVLTVNGP 148
|Q7M2W6|CRYAB_PIG    68 MRLEKDRFSVNLDVKHFSPEELKVKVLGDVIEVHGKHEERQDEHGFISREFHRKYRIPADVDPLTITSSLSSDGVLTVNGP 148
|Q5EWY9|CRYAB_SHEEP  68 VRLEKDRFSVNLDVKHFSPEELKVKVLGDVIEVHGKHEERQDEHGFISREFHRKYRIPADVDPLTITSSLSSDGVLTMNGP 148
|Q05557|CRYAB_ANAPL  67 MRLEKDKFSVNLDVKHFSPEELKVKVLGDMVEIHGKHEERQDEHGFIAREFHRKYRIPADVDPLTITSSLSLDGVLTVSAP 147
|Q05713|CRYAB_CHICK  67 MRLEKDKFSVNLDVKHFSPEELKVKVLGDMIEIHGKHEERQDEHGFIAREFSRKYRIPADVDPLTITSSLSLDGVLTVSAP 147
|Q91312|CRYAB_RANCA  66 MRLEKDKFSINLDVKHFSPEELKVKVSGDFIEIHGKHEERQDEHGYVSRDFQRRYKIPVDVDPLSITSSLSPDGVLTVCGP 146
|P02512|CRYAB_SQUAC  70 LRLDKDKFAIHLDVKHFTPEELRVKILGDFIEVQAQHEERQDEHGYVSREFHRKYKVPAGVDPLVITCSLSADGVLTITGP 150

|P24622|CRYAA_MOUSE  87 VRSDRDKFVIFLDVKHFSPEDLTVKVLEDFVEIHGKHNERQDDHGYISREFHRRYRLPSNVDQSALSCSLSADGMLTFSGP 167
|P02497|CRYAA_MESAU  87 VRSDRDKFVIFLDVKHFSPEDLTVKVLEDFVEIHGKHNERQDDHGYISREFHRRYRLPSNVDQSALSCSLSADGMLTFSGP 167
|P24623|CRYAA_RAT    87 VRSDRDKFVIFLDVKHFSPEDLTVKVLEDFVEIHGKHNERQDDHGYISREFHRRYRLPSNVDQSALSCSLSADGMLTFSGP 167
|P58281|CRYAA_CAVPO  64 VRSDRDKFVIFLDVKHFSPEDLTVKVQEDFVEIHGKHNERQDDHGYISREFHRRYRLPSNVDQSALSCSLSADGMLTFSGP 144
|P02493|CRYAA_RABIT  64 VRSDRDKFVIFLDVKHFSPEDLTVKVQEDFVEIHGKHNERQDDHGYISREFHRRYRLPSNVDQSALSCSLSADGMLTFSGP 144
|P68287|CRYAA_GALCR  64 VRSDRDKFVIFLDVKHFSPEDLTVKVQEDFVEIHGKHNERQDDHGYISREFHRRYRLPSNVDQSALSCSVSADGMLTFSGP 144
|P02470|CRYAA_BOVIN  64 VRSDRDKFVIFLDVKHFSPEDLTVKVQEDFVEIHGKHNERQDDHGYISREFHRRYRLPSNVDQSALSCSLSADGMLTFSGP 144
|P02478|CRYAA_HORSE  64 VRSDRDKFVIFLDVKHFSPEDLTVKVQEDFVEIHGKHNERQDDHGYISREFHRRYRLPSNVDQTALSCSVSADGMLTFSGP 144
|P68280|CRYAA_CANFA  64 VRSDRDKFVIFLDVKHFSPEDLTVKVLEDFVEIHGKHNERQDDHGYISREFHRRYRLPSNVDQSALSCSLSADGMLTFSGP 144
|P68282|CRYAA_FELCA  64 VRSDRDKFVIFLDVKHFSPEDLTVKVLEDFVEIHGKHNERQDDHGYISREFHRRYRLPSNVDQSALSCSLSADGMLTFSGP 144
|P02489|CRYAA_HUMAN  64 VRSDRDKFVIFLDVKHFSPEDLTVKVQDDFVEIHGKHNERQDDHGYISREFHRRYRLPSNVDQSALSCSLSADGMLTFCGP 144
|P02488|CRYAA_MACMU  64 VRSDRDKFVIFLDVKHFSPEDLTVKVQDDFVEIHGKHNERQDDHGYISREFHRRYRLPSNVDQSALSCSLSADGMLTFSGP 143
|P02498|CRYAA_LOXAF  64 VRSDRDQFVILLDVKHFSPEDLTVKVQDDFVEIHGKHNERQDDHGYISREFHRRYRLPSNVDQSALSCSLSADGMLTFCGP 144
|P02502|CRYAA_MACRU  64 VRSDRDKFVIFLDVKHFSPEDLTVKVLDDFVEIHGKHSERQDDHGYISREFHRRYRLPSNVDQSAISCSLSADGMLTFSGP 144
|P02504|CRYAA_CHICK  64 VRSDRDKFTIMLDVKHFSPEDLSVKIIDDFVEIHGKHSERQDDHGYISREFHRRYRLPANVDQSAITCSLSSDGMLTFSGP 144
|P02505|CRYAA_RHEAM  64 VRSDREKFTIMLDVKHFSPEDLSVKIIDDFVEIHGKHSERQDDHGYISREFHRRYRLPSNVDQSAITCSLSSDGMLTFSGP 144
```

Figure S2. Sequence alignment of α-crystallins identify sites for introduction of cysteine.

The core α-domain for 31 α-crystallins from different species were aligned using ClustalW (2), with all cysteine residues highlighted in bold. Cysteine residues are found in only two positions, corresponding to S135 and N146 in human αB-crystallin (red and yellow stripes). These two residues are both on the exterior of the protomer (1, 3, 4). S135 and N146 are thus good candidates for mutation to cysteine and subsequent modification with the MTSL paramagnetic spin label, without causing unwanted structural perturbation.

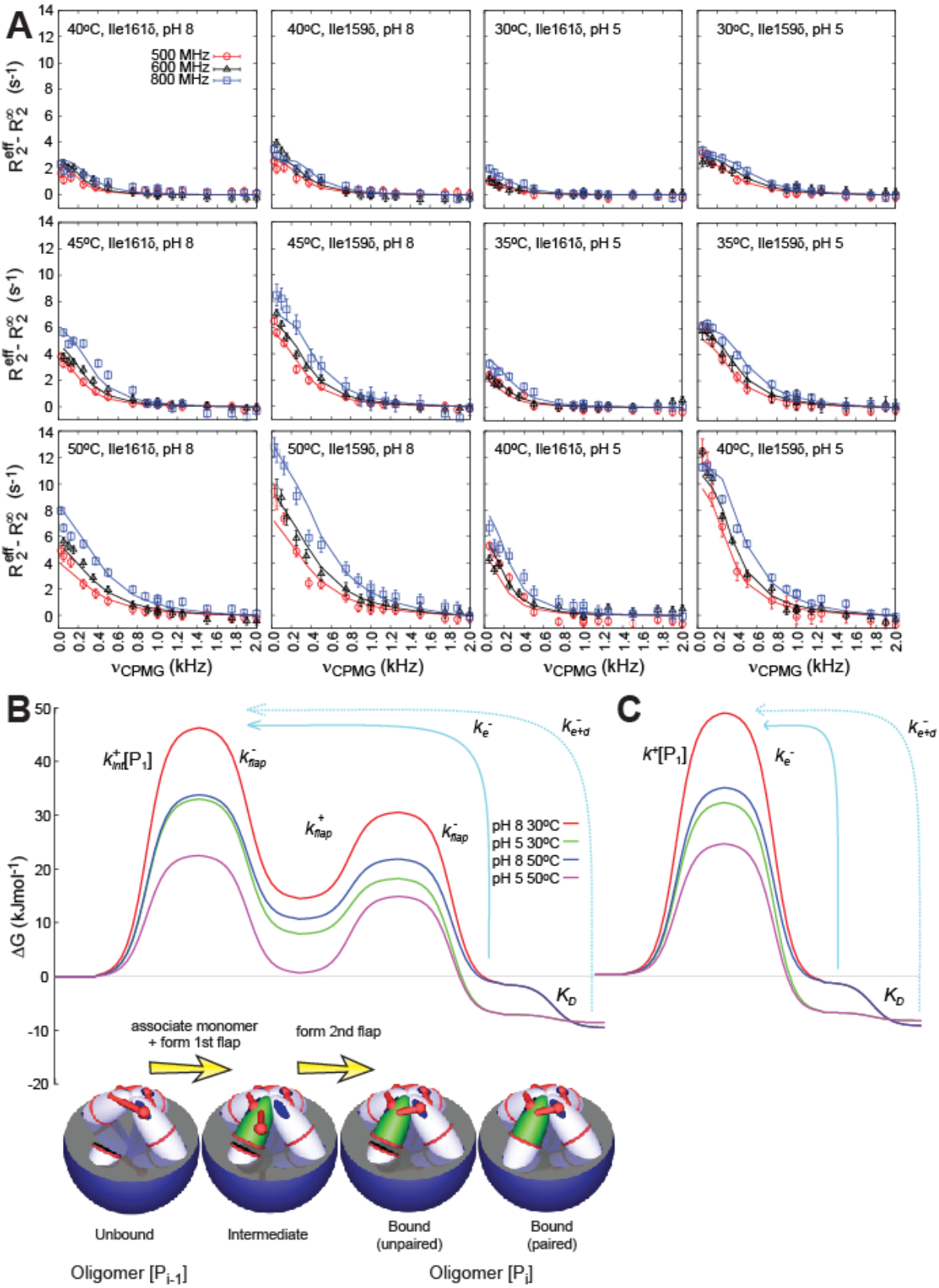

Figure S3. NMR relaxation dispersion measurements probing ms time-scale exchange.

(A) Single quantum methyl ^{13}C CPMG relaxation dispersion curves (5) showing the variation of the exchange contribution to the effective transverse carbon relaxation rate, R_2^{ex}, obtained by taking the difference between the measured R_2^{eff} and the exchange independent intrinsic rate R_2^{∞}, as a function of CPMG pulsing frequency ν_{CPMG}. Data are shown for I159 and I161 at pH 5 and pH 9, and at temperatures between 30°C and 50°C, as individually indicated. (B) The combined mass spectrometry and NMR spectroscopy data allows construction of free energy surfaces describing the association of an αB-crystallin monomer to a growing oligomer at the pH and temperature values indicated. The landscape is constructed using Eqs. given above. (C) The corresponding two state free energy surfaces obtained from using mass spectrometry data alone.

Table S1. Methyl transverse proton relaxation rates, R_2, measured on αB-crystallin cysteine mutant samples, N146C and S135C. Measurements were made for the methyl residues indicated with MTS label, without MTS label and when mixed with unlabelled protein with the mixing ratios [unlabelled/labelled] indicated. The magnitude of the PRE effect is obtained by taking the difference between the +MTSL and –MTSL R_2 rates.

peak	N146 proton R_2 / s^{-1}			S135 proton R_2 / s^{-1}		
	-MTSL	+MTSL	mixed [6/1]	-MTSL	+MTSL	mixed [1/1]
Ile161δ	7.1 ± 1.1	20.7 ± 0.9	10.1 ± 1.3	5.8 ± 1.1	46.7 ± 2.9	26.8 ± 1.6
Ile159δ	6.6 ± 1.2	19.1 ± 1.5	8.4 ± 1.4	5.7 ± 1.1	45.5 ± 3.3	30.8 ± 1.2
Val169γ1	6.9 ± 0.6	16.8 ± 0.4	8.7 ± 0.7	6.7 ± 0.6	36.5 ± 2.4	18.7 ± 0.4
Val169γ2	9.7 ± 0.8	21.7 ± 1.2	10.7 ± 0.8	9.6 ± 0.7	35.3 ± 0.4	20.9 ± 0.9

Table S2. Ground state thermodynamic parameters, activation parameters (denoted by *) and chemical shifts obtained from a global fit of ^{13}C relaxation dispersion profiles (from I159/I161) to a two-state exchange mechanism as described above. The populations of each state and rates of interconversion were assumed to follow Arrhenius behaviour and the chemical shifts were assumed to have a linear temperature dependence. The thermodynamic/activation parameters are defined as $\Delta X_{GE}=X_E-X_G$ (X=H, S) with E and G the excited and ground states respectively.

	pH 5	**pH 9**
ΔH_{GE} (kJ mol^{-1})	123 ± 5	72 ± 20
ΔS_{GE} (J mol^{-1} K^{-1})	357 ± 10	186 ± 20
ΔH_{GE}^* (kJ mol^{-1})	-30.9 ± 0.1	108.5 ± 0.1
ΔS_{GE}^* (Jmol^{-1}K^{-1})	-155 ± 0.1	285.6 ± 0.5
$\lvert\Delta\varpi\rvert$ Ile161δ (ppm) 30°C	1.0 ± 0.4	1.5 ± 0.6
$\lvert\Delta\varpi\rvert$ Ile159δ (ppm) 30°C	2.6 ± 1.0	2.3 ± 0.9

References

1. Laganowsky A*, et al.* (2010) Crystal structures of truncated alphaA and alphaB crystallins reveal structural mechanisms of polydispersity important for eye lens function. *Protein Sci* 19(5):1031-1043
2. Chenna R*, et al.* (2003) Multiple sequence alignment with the Clustal series of programs. *Nucleic Acids Res* 31(13):3497-3500.
3. Bagneris C*, et al.* (2009) Crystal structures of alpha-crystallin domain dimers of alphaB-crystallin and Hsp20. *J Mol Biol* 392(5):1242-1252.
4. Jehle S*, et al.* (2010) Solid-state NMR and SAXS studies provide a structural basis for the activation of alphaB-crystallin oligomers. *Nat Struct Mol Biol* 17(9):1037-1042.
5. Lundstrom P, Vallurupalli P, Religa TL, Dahlquist FW, & Kay LE (2007) A single-quantum methyl 13C-relaxation dispersion experiment with improved sensitivity. *J Biomol NMR* 38(1):79-88.